

Enhanced quantum sensing in time-modulated non-Hermitian systems

Qi-Cheng Wu^{1,*}, Yan-Hui Zhou¹, Tong Liu¹, Yi-Hao Kang², Qi-Ping Su², and Chui-Ping Yang^{2,†}
¹*Quantum Information Research Center and Jiangxi Province Key Laboratory of Applied Optical Technology,
Shangrao Normal University, Shangrao 334001, China*
²*School of Physics, Hangzhou Normal University, Hangzhou 311121, China*

Enhancing the sensitivity of quantum sensing near an exceptional point represents a significant phenomenon in non-Hermitian (NH) systems. However, the application of this property in time-modulated NH systems remains largely unexplored. In this work, we propose two theoretical schemes to achieve enhanced quantum sensing in time-modulated NH systems by leveraging the coalescence of eigenvalues and eigenstates. We conduct a comprehensive analysis of the full energy spectrum, including both real and imaginary components, the population distribution of eigenstates, and various characteristics associated with optimal conditions for sensitivity enhancement. Numerical simulations confirm that eigenvalue-based quantum sensors exhibit a 9.21-fold improvement compared to conventional Hermitian sensors, aligning with the performance of existing time-independent NH sensors. Conversely, for eigenstate-based quantum sensors, the enhancement reaches up to 50 times that of conventional Hermitian sensors, surpassing the results of existing time-independent NH sensors. Moreover, the eigenstate-based sensor exhibits divergent susceptibility even when not close to an exceptional point. Our findings pave the way for advanced sensing in time-sensitive contexts, thereby complementing existing efforts aimed at harnessing the unique properties of open systems.

PACS numbers: 03.67. Pp, 03.67. Mn, 03.67. HK

Keywords: Exceptional point; quantum sensing; susceptibility; non-Hermitian systems

I. INTRODUCTION

Since the discovery of exceptional point (EP) [1–3], a wealth of counterintuitive phenomena and applications have emerged in non-Hermitian (NH) systems [4–9]. In particular, EP-based high-precision sensors play an increasingly crucial role in modern science [10–21]. The unique feature of EP-based sensors is the divergent eigenvalue susceptibility arising from the square-root frequency topology around exceptional points [22, 23], which has been demonstrated in classical optical or electromechanical systems [24–26], trapped ions [27], solid spins [28], single photons [29], or qubit-resonator systems [30]. Recently, several studies have indicated that eigenstate coalescence can also lead to divergent susceptibility in the normalized state population of NH systems, without relying on the existence of EP. For instance, Chu *et al.* proposed a strategy to realize a single-qubit pseudo-Hermitian sensor, which exhibits divergent susceptibility in a dynamical evolution not necessarily involving an EP [31]. Furthermore, Xiao *et al.* introduced and experimentally validated a NH sensing scheme that enhances sensitivity without depending on EP [32]. These schemes offer promising pathways for realizing efficient quantum sensors in NH domains.

Nevertheless, a common assumption in these schemes [10–32] is that the Hamiltonian of the designed sensor is time-independent. In practice, for a broader range of cases, the Hamiltonian of NH systems is time-dependent [33–37], leading to more complex system dynamics. Furthermore, unlike sensors governed by time-independent Hamiltonians, deriving analytical solutions for the dynamic evolution of systems with time-dependent Hamiltonians presents substantial challenges. Consequently, pinpointing parameter intervals that yield optimal sensitivity for estimation purposes becomes considerably more challenging. On the other hand, intuitively, the incorporation of time as an additional degree of freedom markedly enhances the maneuverability of time-dependent NH sensors in comparison to traditional sensors, which may give rise to distinctive effects. Therefore, exploring quantum sensing based on time-dependent NH systems and its potential advantages is highly valuable.

In this work, we introduce an additional temporal dimension to modulate the sensor’s sensitivity to parameter perturbations, thereby bridging the gap between time-independent and time-dependent systems. We propose two theoretical schemes that leverage the coalescence of eigenvalues and eigenstates to achieve enhanced quantum sensing in time-modulated NH systems. A thorough analysis of various features associated with optimal conditions for sensitivity enhancement is conducted, including the optimal timing for achieving high sensitivity using the energy spectrum of eigenvalues and the population distribution of eigenstates. When the time-evolution trajectory of the system approaches the EP, eigenvalue-based quantum sensors exhibit a 9.21-fold improvement over conventional

* E-mail: wuqi.cheng@163.com

† E-mail: yangcp@hznu.edu.cn

Hermitian sensors, aligning with the performance of existing time-independent NH sensors. In contrast, for eigenstate-based quantum sensors, the enhancement reaches up to 50 times that of conventional Hermitian sensors, significantly surpassing the results of existing time-independent NH sensors. Notably, the eigenstate-based sensor continues to display divergent susceptibility even when the time-evolution trajectory of the system deviates from the EP. Our findings open a new avenue for enhanced sensing in time-sensitive frameworks, complementing existing efforts to leverage the unique properties of open systems.

The rest of this paper are organized as follows. In Sec. II, we provide a concise overview of the model for the time-modulated NH sensor. Sections III and IV are dedicated to detailed analyses of the energy spectrum, eigenstate population distribution, and various characteristics associated with optimal conditions for sensitivity enhancement in eigenvalue-based and eigenstate-based quantum sensors, respectively. In Sec. V, we discuss the feasibility of the experimental realization. Finally, we present a summary in Section VI.

II. MODEL OF THE TIME-MODULATED NON-HERMITIAN SENSOR

We consider a generic time-modulated NH qubit sensor subjected to a weak external field. The overall Hamiltonian is expressed as $H = H_S(t) + \lambda H'$, where λ represents the small parameter to be estimated, and H' depends on the form of the weak external field. In an orthonormal basis of states $\{|1\rangle, |0\rangle\}$, the Hamiltonian of the unperturbed time-modulated NH sensor can be expressed as (assuming $\hbar = 1$)

$$H_S(t) = \begin{pmatrix} \epsilon + \delta(t) - \frac{i\gamma_-(t)}{2} & g \\ g & \epsilon - \frac{i\gamma_+(t)}{2} \end{pmatrix}, \quad (1)$$

where $\epsilon + \delta(t)$ and ϵ are the energies of the two levels $|1\rangle$, $|0\rangle$, and g is the interaction strength between the two levels. $\gamma_+(t)$ and $\gamma_-(t)$ are ‘‘gain’’ and ‘‘loss’’ rates (dissipative rates), respectively. When $\gamma_+(t) = \gamma_-(t) = 0$, the NH Hamiltonian $H_S(t)$ reduces to a Hermitian Hamiltonian

$$H_0(t) = \begin{pmatrix} \epsilon + \delta(t) & g \\ g & \epsilon \end{pmatrix}. \quad (2)$$

After performing algebraic calculations, one can find that the eigenvalues of the NH Hamiltonian $H_S(t)$ are

$$E_{\pm}(t) = \frac{1}{4}[2(2\epsilon + \delta(t)) - i(\gamma_+(t) + \gamma_-(t)) \pm 2\Delta_E(t)], \quad (3)$$

with

$$\Delta_E(t) = \frac{i}{2}\sqrt{[\gamma_-(t) - \gamma_+(t) + 2i\delta(t)]^2 - 16g^2}. \quad (4)$$

The corresponding right eigenvectors are

$$\begin{aligned} |\phi_+(t)\rangle &= \frac{1}{S_+(t)}[A_+(t), 4g]^T, \\ |\phi_-(t)\rangle &= \frac{1}{S_-(t)}[A_-(t), 4g]^T, \end{aligned} \quad (5)$$

where $A_{\pm}(t) = 2\delta(t) - i[\gamma_-(t) - \gamma_+(t)] \pm 2\Delta_E(t)$ and $S_{\pm}(t) = \sqrt{|A_{\pm}(t)|^2 + |4g|^2}$, together with the left eigenvectors

$$\begin{aligned} \langle \widehat{\phi}_+(t) | &= \frac{1}{S_+(t)}[A_+(t), 4g], \\ \langle \widehat{\phi}_-(t) | &= \frac{1}{S_-(t)}[A_-(t), 4g]. \end{aligned} \quad (6)$$

The biorthogonal partners $\{\langle \widehat{\phi}_n | \}, \{|\phi_m\rangle\}$ ($n, m = +, -$) are normalized to satisfy the biorthogonality and closed relations $\langle \widehat{\phi}_n(t) | \phi_m(t) \rangle = \delta_{nm}$, $\sum_n |\widehat{\phi}_n(t)\rangle \langle \phi_n(t)| = \sum_n |\phi_n(t)\rangle \langle \widehat{\phi}_n(t)| = 1$ [7].

III. EIGENVALUE-BASED QUANTUM SENSING

Without loss of generality, the form of the perturbation Hamiltonian H' can be set as $H' = \sigma_x$, and the estimated parameter λ can be considered as deviations of the interaction strength g . In this section, we will propose a theoretical framework for eigenvalue-based quantum sensing to detect minute deviations λ of the interaction strength g from its normal value g_0 , defined as $\lambda = g - g_0$.

Based on Eq. (4), the derivative of the energy splitting $\Delta_E(t)$ to the parameter g at time t (i.e., the susceptibility of the quantum sensor) is

$$\chi(t) = \frac{\partial \Delta_E(t)}{\partial g} = \frac{4g}{\Delta_E(t)}, \quad (7)$$

which diverges under an eigenenergy-matching condition [$\Delta_E(t) \rightarrow 0$ near EP or diabolic point (DP)]. This divergent behavior implies that even a small variation of g causes a significant change of the energy splitting around the EP or DP at time t .

It is important to note that in NH systems, the energy splitting $\Delta_E(t)$ is generally a complex quantity. However, when $\gamma_+(t) = \gamma_-(t) = 0$, the Hermitian Hamiltonian $H_0(t)$ causes $\Delta_E(t)$ to become a real quantity. To uniformly evaluate the performance of the quantum sensor in both Hermitian and NH regimes, we characterize the non-Hermiticity-enabled sensitivity enhancement by

$$S_E(t) = \left| \frac{\chi_{NH}(t)}{\chi_H(t)} \right|, \quad (8)$$

where $\chi_H(t)$ and $\chi_{NH}(t)$ are the susceptibility of the quantum sensor in Hermitian and NH regimes, respectively.

A. Optimal time window for achieving high sensitivity

Unlike quantum sensors based on time-independent systems, those based on time-dependent systems introduce an additional temporal dimension that enables the regulation of sensitivity to parameter perturbations. A comprehensive investigation into the optimal time window for achieving high sensitivity is crucial. For the sake of discussion, we assume $\gamma_+(t) = \alpha\gamma_-(t)$ and normalize all parameters with respect to the energy scale ϵ in the following analysis. The analysis of Eq. (4) reveals that exceptional points (EPs) occur under two conditions: (i) when $\delta = g = \gamma_- = 0$, and (ii) when $\delta = 0$, $\alpha = -1$ and $2g = |\gamma_-| \neq 0$. In both cases, the energy discriminant $\Delta_E(\delta, g, \gamma_-)$ equals zero. However, simultaneously analyzing the relationship between the time-dependent parameters [$\delta(t), g, \gamma_-(t)$] and $\Delta_E(t)$ poses a considerable challenge. Therefore, it is advisable to fix certain parameters and conduct an in-depth investigation into the correlation between the remaining parameters and $\Delta_E(t)$.

Theoretically, $\Delta_E(t)$ can be rewritten as

$$\Delta_E(t) = \rho(t) \exp\left(\frac{i[\theta(t) + \pi]}{2}\right), \quad (9)$$

with

$$\begin{aligned} \rho^2(t) &= [c(t) - a(t)]^2 + 2b(t)[c(t) - a(t)] + b^2(t) + 4a(t)b(t), \\ \theta(t) &= \arctan\left[\frac{2\sqrt{a(t)b(t)}}{a(t) - b(t) - c(t)}\right], \end{aligned} \quad (10)$$

where $a(t) = (1 - \alpha)^2\gamma_-^2(t)$, $b(t) = 4\delta^2(t)$, and $c(t) = 16g^2$. Then, the eigenvalue-matching condition $\Delta_E(t) \rightarrow 0$ can be equivalently transformed into the condition $\rho^2(t) \rightarrow 0$. From Eq. (10), it is evident that $\rho^2(t)$ can be expressed as a time-dependent parabola with an upward opening. To analyze the impact of changes in the parameter g on $\rho^2(t)$, we consider $c(t) - a(t)$ as a variable. Consequently, $\rho^2(t)$ attains its minimum value $\rho^2(\tau)_{\min}$ at time τ , where $c(\tau) - a(\tau) = -b(\tau)$. We emphasize that $|\rho(\tau)|_{\min} = 0$ implies $\Delta_E(\tau) = 0$, indicating that the system is at an EP or DP. Consequently, $|\rho(\tau)|_{\min}$ can serve as a quantitative measure to evaluate the deviation of the system's parameter trajectory from the EP or DP.

In addition, if $c(t)$ is a positive constant coefficient c and $0 < c \leq \max[a(t) - b(t)]$, the existence of an optimal time τ ,

$$c = [a(\tau) - b(\tau)], \quad (11)$$

can be guaranteed, ensuring high sensitivity of $\rho^2(t)$ to changes in the parameter c . However, if $c > \max[a(t) - b(t)]$, the relationship $c - a(\tau) = -b(\tau)$ cannot hold. In this scenario, a notably high sensitivity of $\rho^2(t)$ to variations in the parameter c remains evident when

$$|a(\tau) - b(\tau)| = \max[a(t) - b(t)]. \quad (12)$$

It is important to note that when the parameter c becomes significantly large, the trajectory of the system parameter change deviates substantially from the EP, resulting in $|\rho(\tau)|_{\min} \gg 0$. Consequently, the eigenvalue-matching condition no longer holds, leading to a rapid decrease in the susceptibility of the quantum sensor as c increases. Therefore, if the forms of $a(t)$ and $b(t)$ are fixed, for the interaction strength g , there exists a trade-off between achieving high sensitivity [as shown in Eq. (7), where $\chi(t)$ is proportional to g] and maintaining the eigenvalue-matching condition over time [$0 < 16g^2 < \max|a(t) - b(t)|$].

B. Performance of eigenvalue-based quantum sensing

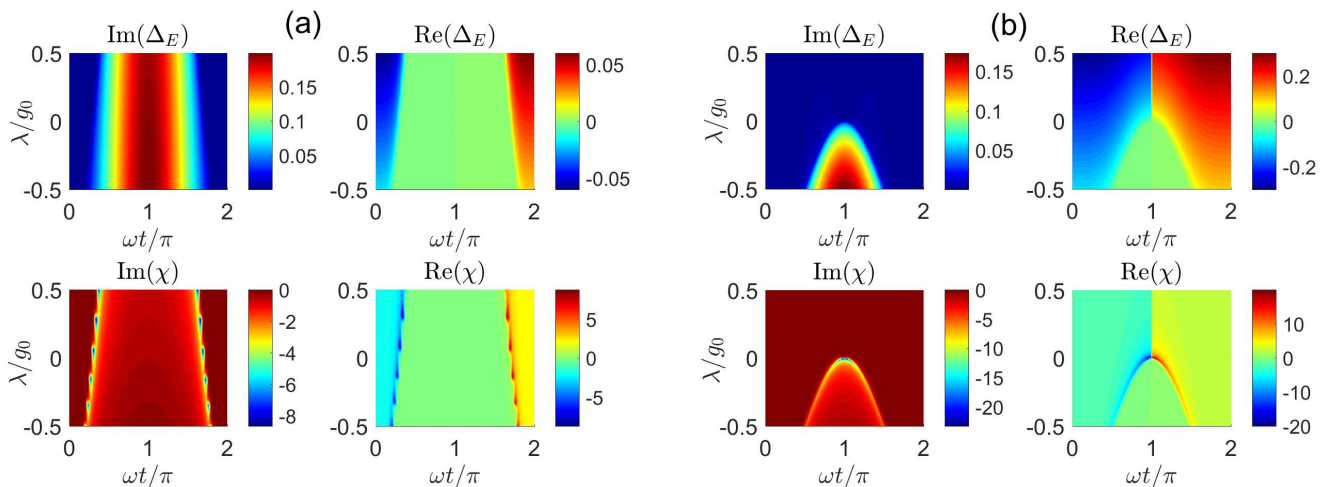


FIG. 1: The real and imaginary parts of the energy splitting $\Delta_E(t)$ and the susceptibility $\chi(t)$ as functions of λ/g_0 and $\omega t/\pi$ for the NH sensor. In panels (a) and (b), the interaction strength g_0 is set to 0.02 and 0.1, respectively. Other parameters are fixed at $\Delta_0 = 0.04$, $\alpha = -1$, and $\Gamma_0 = 0.2$.

To gain a more intuitive understanding of the aforementioned results, let us examine a time-modulated parameter trajectory [38, 39]

$$g = g_0, \delta(t) = \Delta_0 \sin(\omega t), \gamma_-(t) = \Gamma_0 \sin^2\left(\frac{\omega t}{2}\right), \quad (13)$$

where $g_0, \Delta_0, \Gamma_0, \omega \in \mathbf{R}$ are constants, the period of the trajectory is $T = 2\pi/\omega$. To assess the validity of eigenvalue-based quantum sensing, we investigate the time-dependent behavior of the complex parameters (i.e., the energy splitting $\Delta_E(t)$ and the susceptibility $\chi(t)$) by analyzing the influence of the perturbation λ/g_0 .

As illustrated in Fig. 1(a), both the real and imaginary components of the energy splitting Δ_E exhibit non-monotonic variations, characterized by abrupt transitions at specific intervals (from blue to green, and from green to red). Correspondingly, sensitivity peaks for $\text{Im}(\chi)$ are observed in the deep blue region; while for $\text{Re}(\chi)$, they occur in both the deep blue and red regions. This divergent behavior indicates that a minor variation in λ/g_0 can lead to significant changes in the splitting at specific times τ . Consequently, by selecting appropriate time nodes, we can achieve optimal sensitivity detection for different disturbances $\lambda/g_0 \approx \Delta_g$ (where Δ_g is an arbitrary constant coefficient). Alternatively, we can finely adjust the magnitude of g_0 so that the sensitivity peak occurs when $\lambda/g_0 \approx 0$ for a fixed time. Similarly, as illustrated in Fig. 1(b), when $g_0 = 0.1$, the energy splitting Δ_E undergoes a phase transition at the point $(\lambda/g_0 = 0, t = \pi/\omega)$. At this critical point, sensitivity peaks with $|\text{Im}(\chi)| \approx 22$ and $|\text{Re}(\chi)| \approx 20$ are also observed.

Next, we investigate the energy splitting $|\Delta_E(t)|$ and the susceptibility $|\chi_{NH}(\tau)|$ [$|\chi_H(\tau)|$] for both the NH sensor and its Hermitian counterpart under varying parameters. For the NH sensor, the time-dependent functions $\delta(t)$

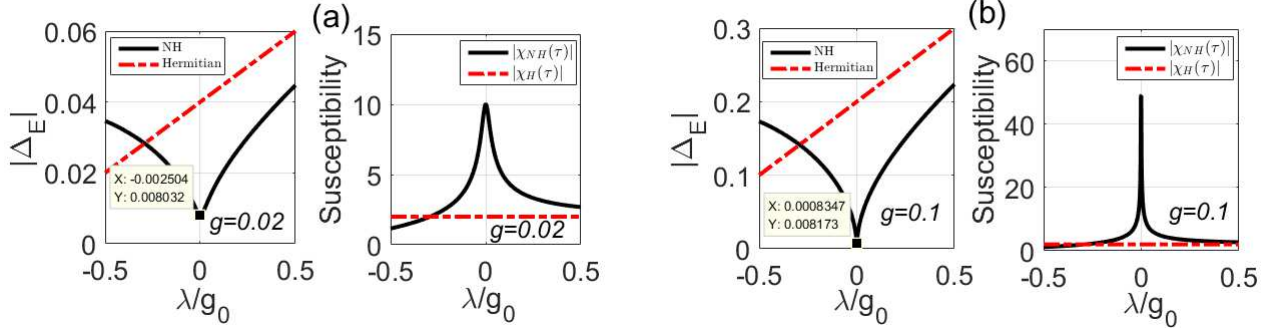


FIG. 2: The energy splitting $\Delta_E(\tau)$ and the susceptibility $|\chi_{NH}(\tau)|$ [$|\chi_H(\tau)|$] as functions of λ/g_0 for the NH sensor (solid black line) and its Hermitian counterpart (dotted red line), respectively. The interaction strength g_0 and the selected time τ are chosen as 0.02 and $0.295\pi/\omega$ in panel (a), while 0.1 and π/ω in panel (b) according to Eq. (11). Other parameters are set as follows: $\Delta_0 = 0.04$, $\alpha = -1$, $\Gamma_0 = 0.2$ for the NH sensor, and $\Gamma_0 = 0$ for the Hermitian sensor.

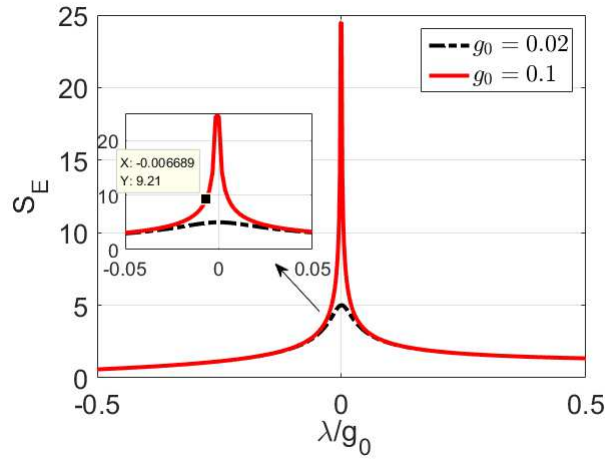


FIG. 3: The sensitivity enhancement S_E , enabled by non-Hermiticity, as a function of λ/g_0 for the NH sensor. The other parameters remain consistent with those in Fig. 2.

and $\gamma(t)$ are, respectively, defined as $\delta(t) = 0.04 \sin(\omega t)$ and $\gamma(t) = 0.2 \sin^2(\frac{\omega t}{2})$ for simplicity. In contrast, for the Hermitian sensor, $\delta(t) = 0.04 \sin(\omega t)$ but $\gamma(t) = 0$. Figure 2 illustrates the energy splitting $|\Delta_E(t)|$ and the susceptibility $|\chi_{NH}(\tau)|$ [$|\chi_H(\tau)|$] as functions of λ/g_0 for both the NH sensor (solid black line) and its Hermitian counterpart (dotted red line).

As illustrated in Figs. 2(a) and 2(b), when $g_0 = 0.02$ and $g_0 = 0.1$, which are relatively small values ($0 < c \leq \max[a(t) - b(t)]$), the eigenvalue-matching condition for the NH sensor is satisfied. This results in a minimum energy splitting of $|\Delta_E(\tau)|_{\min} \approx 8.03 \times 10^{-3}$ for $g_0 = 0.02$ at $\tau = 0.295\pi/\omega$ and $|\Delta_E(\tau)|_{\min} \approx 8.17 \times 10^{-3}$ for $g_0 = 0.1$ at $\tau = \pi/\omega$, during one period. Therefore, even a smaller deviation of the interaction strength g from g_0 leads to enhanced sensitivity $|\chi_{EP}(\tau)|$ in both Figs. 2(a) and 2(b). However, the sensitivity peak illustrated in Fig. 2(b) surpasses that in Fig. 2(a), attributed to the higher fixed parameter value $g_0 = 0.1$ in Fig. 2(b). On the other hand, under the Hermitian mechanism, as illustrated in Figs. 2(a) and 2(b), the system's sensitivity $|\chi_H(\tau)|$ remains nearly invariant regardless of variations in the parameter λ/g_0 . This is irrespective of whether the eigenvalue-matching condition is fulfilled. Hence, it can be concluded that, in the NH scenario, the eigenenergy exhibits sharper variations with respect to small changes in λ/g_0 compared to its Hermitian counterpart.

To intuitively compare the enhanced sensitivity achieved using EP with that achieved using conventionally DP in quantum sensing, we investigate the non-Hermiticity-enabled sensitivity enhancement factor S_E . For small values of g_0 [e.g., $g_0 = 0.02$ and $g_0 = 0.1$], the sensitivity enhancement factor S_E increases monotonically as $|\lambda/g_0|$ decreases. Ideally, this enhancement can reach up to 9.21 when the deviation $|\lambda/g_0| = 0.006689$ (see the red lines in Fig. 3). This finding aligns with the performance of existing time-independent NH sensors [28, 30–32], demonstrating that NH sensors offer a significant advantage over conventional Hermitian sensors in estimating λ .

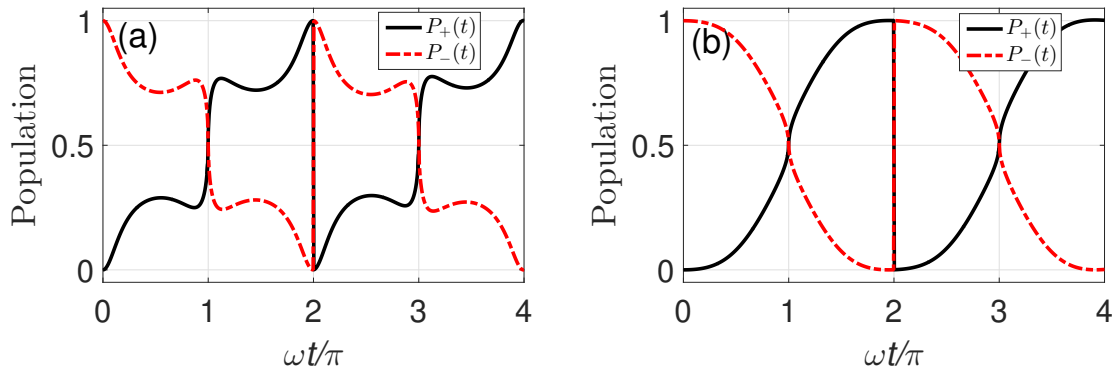


FIG. 4: The time evolution of the normalized population $P_m(t)$ for the time-dependent right eigenstate $|\phi_m(t)\rangle$ ($m = +, -$). The initial state is chosen as $|\Psi(0)\rangle = |\phi_-(0)\rangle$. In panel (a), the parameters are set to $g_0 = 0.01$, $\Delta_0 = 0.04$, $\Gamma_0 = 0.02$, $\omega = \pi$, and $\alpha = -1$, while in panel (b), they are set to $g_0 = 0.02$, $\Delta_0 = 0.01$, $\Gamma_0 = 0.04$, $\omega = \pi$, and $\alpha = -1$. The population of the system experiences a rapid inversion when $\omega t/\pi \approx j$ ($j \in \mathbf{Z}^+$).

IV. EIGENSTATE-BASED QUANTUM SENSING

Recent studies have demonstrated that asymmetric (chiral) state transfer can be achieved by tuning system parameters along a path encircling an EP or an approximate exceptional point [37–45]. During this quantum state transformation, the eigenstate populations of the system undergo rapid change at a specific time. This feature is significant because it indicates that abrupt shifts in the population of eigenstates, in time-dependent systems, can serve as indirect but accurate indicators of changes in system parameters. In this work, we aim to determine the optimal range of parameter sensitivity in time-dependent NH sensors through numerical analysis of system population dynamics. Additionally, we propose a theoretical framework for eigenstate-based quantum sensing to detect subtle deviations in the interaction strength.

A. The optimal time window for achieving high sensitivity

We first focus on the unperturbed system dynamics governed by $H_S(t)$ with the sensor initialized in one of its right eigenstates, i.e., $|\Psi(0)\rangle = |\phi_+(0)\rangle$. Generally, the evolving state $|\Psi(t)\rangle$ can be obtained by numerically calculating the following Schrödinger's equation

$$i\partial_t|\Psi(t)\rangle = H_S(t)|\Psi(t)\rangle. \quad (14)$$

As shown in Refs. [37–45], efficient asymmetric or symmetric state transfers can be realized by modulating system parameters. Specifically, an asymmetric state transfer can be achieved via a carefully designed parameter trajectory, such as the system time-evolution trajectory illustrated in Eq. (13). To evaluate the optimal time window for achieving high sensitivity, we investigate the temporal dynamics of the system. The normalized population of the right eigenstate $|\phi_m(t)\rangle$ ($m = +, -$) is determined by the following relation

$$P_m(t) = \frac{|\langle \widehat{\phi}_m(t) | \Psi(t) \rangle|^2}{|\langle \widehat{\phi}_+(t) | \Psi(t) \rangle|^2 + |\langle \widehat{\phi}_-(t) | \Psi(t) \rangle|^2}, \quad (15)$$

where $|\Psi(t)\rangle$ represents the evolving state of the system at time t .

In Fig. 4, we illustrate the temporal evolution of the population $P_m(t)$ for the right eigenstate $|\phi_m(t)\rangle$ ($m = +, -$) under two sets of parameters near the EP. Specifically, Fig. 4(a) corresponds to the parameters $g_0 = 0.01$, $\Delta_0 = 0.04$, $\Gamma_0 = 0.02$, $\omega = \pi$, and $\alpha = -1$, while Fig. 4(b) uses $g_0 = 0.02$, $\Delta_0 = 0.01$, $\Gamma_0 = 0.04$, $\omega = \pi$, and $\alpha = -1$. It is observed that when $\omega t/\pi \approx j$ ($j \in \mathbf{Z}^+$), the population $P_m(t)$ undergoes a rapid inversion. Notably, a small deviation Δt from the fixed time $t_0 \approx j\pi/\omega$ results in a significant change in the population. Consequently, the population signal described by Eq. (15) exhibits high sensitivity to variations in time t . On the other hand, at the specific time $t_0 \approx j\pi/\omega$, the parameters defined in Eq. (13) are fixed as follows: $g = g_0$, $\delta(t_0) = 0$, and $\gamma_-(t_0) = \Gamma_0 \sin^2(j\pi/2)$. A small deviation Δt from this fixed time t_0 leads to correspondingly small deviations in these parameters. This phenomenon is significant because it allows for the indirect but precise determination of parameter changes by analyzing abrupt

shifts in the quantum state population of time-dependent systems. Consequently, this system can serve as an efficient sensor for detecting variations in the fixed parameters $[g, \delta(t_0), \gamma_-(t_0)]$.

It is crucial to emphasize that two distinct physical mechanisms are involved in the entire dynamic process. (i) The nontrivial population conversion, characterized by rapid population coalescence within half a period as illustrated in Fig. 4, originates from dynamically varying system parameters along a path enclosing an EP. This phenomenon is a unique attribute of non-Hermitian systems. (ii) The trivial population conversion, where the state transformation occurs over one full period, results from dynamically varying system parameters along a path enclosing a DP, which is a common feature of Hermitian systems. Specifically, the system functions as a NH sensor when $\omega t/\pi \approx 2k - 1$ (where $k \in \mathbf{Z}^+$ and the dissipative parameter $\gamma_-(t_0) = \Gamma_0$), or as a Hermitian sensor when $\omega t/\pi \approx 2k$ (where $k \in \mathbf{Z}^+$ and the dissipative parameter $\gamma_-(t_0) = 0$). Consequently, the time-modulated quantum sensor exhibits differential sensitivities to changes in the fixed parameters $[g(t_0), \delta(t_0), \gamma_-(t_0)]$.

Without loss of generality, we still assume that the parameter g deviates slightly from its fixed value g_0 , such that $\lambda = g - g_0$ represents the deviation. Then, according to Eq. (6), the perturbed left eigenvectors can thus be expressed as

$$\begin{aligned} \langle \widehat{\phi}_+(t, \lambda) | &= \frac{1}{S_+(t, \lambda)} \{A_+(t, \lambda), 4g(\lambda)\}, \\ \langle \widehat{\phi}_-(t, \lambda) | &= \frac{1}{S_-(t, \lambda)} \{A_-(t, \lambda), 4g(\lambda)\}, \end{aligned} \quad (16)$$

where $S_{\pm}(t, \lambda) = \sqrt{|A_{\pm}(t, \lambda)|^2 + |4g(\lambda)|^2}$, $A_{\pm}(t, \lambda) = 2\delta(\tau) - i[\gamma_-(\tau) - \gamma_+(\tau)] \pm 2\Delta_E(t, \lambda)$, and $\Delta_E(t, \lambda) = \frac{i}{2}\sqrt{[\gamma_-(\tau) - \gamma_+(\tau) + 2i\delta(\tau)]^2 - 16g(\lambda)^2}$.

The normalized population of the right eigenstate $|\phi_m(\tau)\rangle$ ($m=+, -$) is determined by the relation

$$P_m(t, \lambda) = \frac{|\langle \widehat{\phi}_m(t, \lambda) | \Psi(t) \rangle|^2}{|\langle \widehat{\phi}_+(t, \lambda) | \Psi(t) \rangle|^2 + |\langle \widehat{\phi}_-(t, \lambda) | \Psi(t) \rangle|^2}. \quad (17)$$

Based on the outcomes of the measurements on the sensor system, one can derive the susceptibility

$$\chi(t, \lambda) = \frac{\partial P_+(t, \lambda)}{\partial \lambda} = \frac{P_+(t, \lambda_{i+1}) - P_+(t, \lambda_i)}{\lambda_{i+1} - \lambda_i}, \quad (18)$$

where the subscript i denotes the data index. Eq. (18) quantifies the sensitivity of the population $P_+(t, \lambda)$ to changes in the parameter λ for a given evolution time t . To uniformly evaluate the performance of the quantum sensor in both Hermitian and NH regimes, we further characterize the sensitivity enhancement enabled by non-Hermiticity as

$$S_P(t, \lambda) = \left| \frac{\chi_{NH}(t, \lambda)}{\chi_H(t, \lambda)} \right|, \quad (19)$$

where $\chi_{NH}(t)$ and $\chi_H(t)$ are the susceptibility of the quantum sensor in Hermitian and NH regimes, respectively.

B. Performance of eigenstate-based quantum sensing

In section IVA, we propose that the phenomenon of rapid inversion of the eigenstate population when $\omega t/\pi \approx j$ ($j \in \mathbf{Z}^+$), as illustrated in Fig. 4, can be harnessed to achieve high sensitivity in quantum sensing. Moreover, the sensitivities of the sensors exhibit distinct behaviors: for the NH sensor, the sensitivity peaks when $\omega t/\pi \approx 2k - 1$, while for the Hermitian sensor, it peaks when $\omega t/\pi \approx 2k$. To more rigorously validate this hypothesis, we examine the behavior of the normalized population $P_+(\tau)$ of the right eigenstate $|\phi_+(\tau)\rangle$ and the susceptibility $\chi(\tau)$ of the NH sensor, as shown in Fig. 5. Here, we use two sets of parameters near the EP, which have been discussed in Fig. 4.

One can observe that when λ/g_0 is fixed at a value such as 0.1, the normalized population $P_+(t, \lambda)$ in Figs. 5(a) and 5(b) undergoes rapid inversions near the times $\omega t/\pi \approx 1, 2, 3$. Additionally, for the times $\omega t/\pi \approx 1, 3$, the normalized population $P_+(t, \lambda)$ exhibits sharp changes near $\lambda/g_0 = 0$. Correspondingly, the sensitivity $\chi(t, \lambda)$ also shows significant variations near $\lambda/g_0 = 0$ at these times. However, at $\omega t/\pi \approx 2$, which is expected to enable high-sensitivity detection, this expectation is not met. Despite the rapid inversion of $P_+(t, \lambda)$ at $\omega t/\pi \approx 2$, the sensitivity $\chi(t, \lambda)$ remains very small and nearly invariant with respect to λ/g_0 . Consequently, for a NH sensor, the susceptibility signal described by Eq. (19) exhibits high sensitivity to changes in λ/g_0 only when $\omega t/\pi \approx 2k - 1$ for $k \in \mathbf{Z}^+$.

To gain an intuitive understanding of the behavior of the normalized population $P_+(\tau)$ and the susceptibility $\chi(\tau)$ at several time points near $t \approx \pi/\omega$ ($\tau = 0.96\pi/\omega, 0.98\pi/\omega, 1.02\pi/\omega, 1.04\pi/\omega$), we present the results in Fig. 6. As

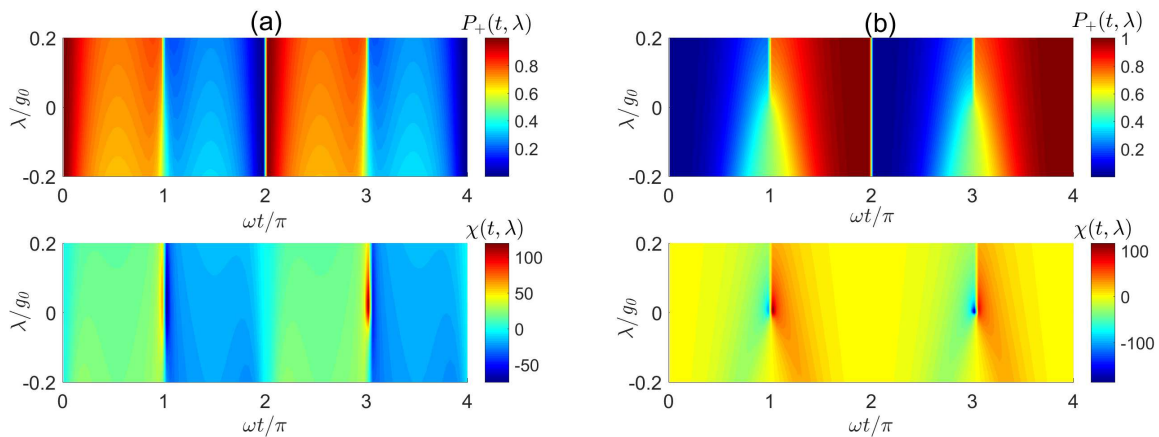


FIG. 5: The normalized population $P_+(t, \lambda)$ of the right eigenstate $|\phi_+(t, \lambda)\rangle$ and the susceptibility $\chi(t, \lambda)$ of the NH sensor as functions of λ/g_0 at different times. In panel (a), the parameters are set to $g_0 = 0.01$, $\Delta_0 = 0.04$, $\Gamma_0 = 0.02$, $\omega = \pi$, and $\alpha = -1$, while in panel (b), they are set to $g_0 = 0.02$, $\Delta_0 = 0.01$, $\Gamma_0 = 0.04$, $\omega = \pi$, and $\alpha = -1$. The susceptibility $\chi(t, \lambda)$ exhibits extremely sharp peaks near $\omega t/\pi \approx 2k - 1$ where $k \in \mathbf{Z}^+$.

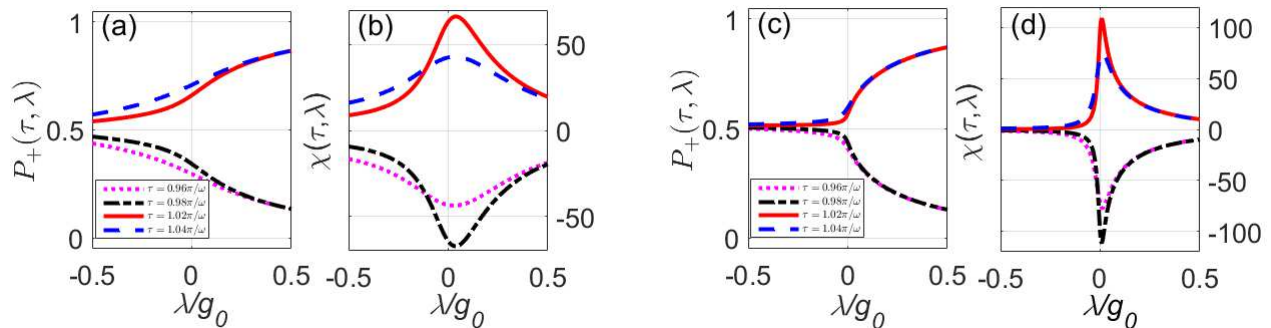


FIG. 6: The normalized population $P_+(\tau)$ of the right eigenstate $|\phi_+(\tau)\rangle$ and the susceptibility $\chi(\tau)$ of the NH sensor as functions of λ/g_0 at different times. In panels (a) and (b), the parameters are set to $g_0 = 0.01$, $\Delta_0 = 0.04$, $\Gamma_0 = 0.02$, $\omega = \pi$, and $\alpha = -1$, while in panels (c) and (d), the parameters are set to $g_0 = 0.02$, $\Delta_0 = 0.01$, $\Gamma_0 = 0.04$, $\omega = \pi$, and $\alpha = -1$.

illustrated in Fig. 6(a), the normalized population $P_+(\tau)$ exhibits rapid fluctuations across all selected time nodes as λ/g_0 varies. Correspondingly, in Fig. 6(b), the magnitude of the susceptibility $|\chi(\tau)|$ increases sharply with decreasing $|\lambda/g_0|$. By comparing the sensitivity variations at different time nodes, it is evident that a smaller time offset leads to a higher peak value of $|\chi(\tau)|$. Similar trends are observed in Figs. 6(c) and 6(d). Notably, when comparing Fig. 6(b) and Fig. 6(d), it is found that under identical measurement times, the peak value of $|\chi(\tau)|$ in Fig. 6(d) is higher than in Fig. 6(b), albeit with slightly reduced broadening. These observations substantiate the feasibility and efficiency of our proposed quantum sensor based on population dynamics.

We present the non-Hermiticity-enabled sensitivity enhancement factor S_P as a function of λ/g_0 and t in Fig. 7. It is observed that the sensitivity enhancement factor $|S_P|$ is significantly large and increases approximately monotonically as $|\lambda/g_0|$ decreases under both sets of parameter conditions. Specifically, for the parameter condition with $g_0 = 0.01$, the peak value of S_P reaches approximately 100. Moreover, S_P remains greater than 50 when $\lambda/g_0 > -0.06187$, surpassing the performance of conventional Hermitian sensors and existing time-independent NH sensors [28, 30–32].

V. FEASIBILITY OF THE EXPERIMENTAL REALIZATION

Our proposal can be realized in various physical settings, which necessitates the engineering of the single-qubit Hamiltonian described by Eq. (1). For instance, it can be implemented in a system of two coupled dissipative cavities [37, 46–48], where $\gamma_+(t)$ [$\gamma_-(t)$] denotes the cavity gain (loss) rate and $\delta(t)$ is the frequency detuning of the cavities. The cavities are coupled coherently with interaction strength g , while λ accounts for deviations of the

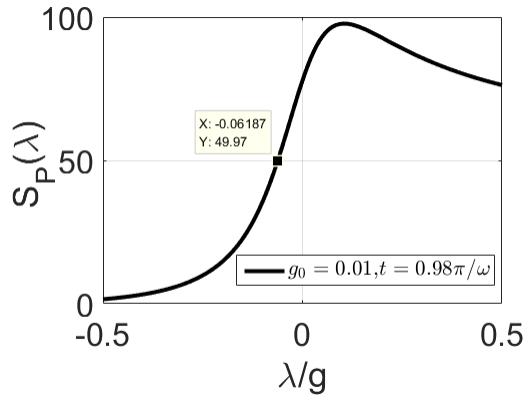


FIG. 7: The sensitivity enhancement enabled by non-Hermiticity of the sensor is investigated as a function of λ/g_0 . For the Hermitian (NH) sensor, the dissipation factor is chosen as $\Gamma_0 = 0$ ($\Gamma_0 = 0.02$). Other parameters are set as follows: $t = 0.98\pi/\omega$, $g_0 = 0.01$, $\Delta_0 = 0.04$, $\omega = \pi$, and $\alpha = -1$.

interaction strength g due to a weak external field. Specifically, for a whispering-gallery microcavity, such as a micro-disk or micro-toroid, under the two-mode approximation of counter-traveling waves and perturbed by N Rayleigh scatterers [46–48], the effective Hamiltonian in the traveling-wave basis (counterclockwise and clockwise) is

$$H^{(N)} = \begin{pmatrix} \omega^{(N)} & A^{(N)} \\ B^{(N)} & \omega^{(N)} \end{pmatrix}, \quad (20)$$

where $\omega^{(N)} = \omega_0 + \sum_{j=1}^N \varepsilon_j$, $A^{(N)} = \sum_{j=1}^N \varepsilon_j e^{-i2m\beta_j}$ and $B^{(N)} = \sum_{j=1}^N \varepsilon_j e^{i2m\beta_j}$. Here, m is the azimuthal mode number, ω_0 is the complex frequency of the unperturbed resonance mode, β_j is the angular position of scatterer j , and ε_j is the complex frequency splitting that is introduced by scatterer j alone. It is possible for $|A^{(M)}|$ to differ from $|B^{(M)}|$, due to the asymmetry in backscattering between clockwise- and anticlockwise-travelling waves. Notably, the above Hamiltonian is still non-Hermitian because ε_j and ω_0 are complex numbers that reflect the presence of losses [46]. The Hamiltonian in Eq. (1) can also be realized in other physical systems, such as solid-state spin in diamond and superconducting qubit for magnetic field and microwave detection. In particular, the implementation of NH dynamics has been achieved using a nitrogen-vacancy center in diamond through selective microwave pulses [49]. In addition, it has been achieved in a single-photon interferometric network [50]. This further facilitates the experimental realization of the present proposal.

Moreover, the feasibility of obtaining key information through actual quantum measurements is a critical factor for enhancing the sensitivity of quantum sensing in experimental contexts. For eigenvalue-based quantum sensors, the sensitivity of quantum sensing relies on the precise measurement of the energy splitting Δ_E . Fortunately, recent experiments have demonstrated that the real part of the energy splitting $\text{Re}(\Delta_E)$ corresponds to the conventional frequency splitting, while the imaginary part $\text{Im}(\Delta_E)$ determines the linewidth. Both frequency splitting and linewidth can be accurately measured experimentally in a whispering-gallery microcavity (for details, see Refs. [13, 24, 46, 51–53]). Furthermore, from an experimental perspective, based on the specific experimental parameters, precisely measuring either the frequency splitting or the linewidth is sufficient to achieve enhanced sensitivity. For instance, as shown in Fig. 1(a), although the sensor sensitivities obtained by measuring the real and imaginary parts are not significantly different, it is evident that the imaginary part $\text{Im}(\Delta_E)$ is substantially larger than its real part $\text{Re}(\Delta_E)$. In this case, choosing to measure the imaginary part, i.e., the linewidth of the system, is more practical and reasonable experimentally. Similarly, under the system parameters illustrated in Fig. 1(b), selecting to measure the frequency splitting in the system is more advisable for achieving higher sensor sensitivity.

On the other hand, for the eigenstate-based quantum sensor, the sensitivity of quantum sensing depends on the precise measurement of the population of the right eigenstate $P_m(t, \lambda)$ ($m = +, -$). It should be noted that accurately measuring the population of the eigenstate at the EP poses significant experimental challenges. This is because the eigenstates of non-Hermitian systems become identical at the EP, and due to their indistinguishability in non-Hermitian systems, determining the population of the eigenstate becomes difficult. Fortunately, the technique for quantum state discrimination has been extensively studied [54, 55] and has already been experimentally realized in recent studies within non-Hermitian systems [56, 57]. Moreover, one can also choose to appropriately deviate the system parameter trajectory from the EP, thereby enhancing the distinguishability between eigenstates and alleviating the experimental challenge associated with measuring the population of eigenstates. In fact, as shown in

the Appendix A, the eigenstate-based sensor still exhibits significant susceptibility during dynamical evolution, even when not close to an EP.

VI. CONCLUSION

We have proposed two theoretical schemes to achieve enhanced quantum sensing in time-modulated non-Hermitian systems by leveraging the coalescence of eigenvalues and eigenstates. This approach contrasts sharply with previous studies, where the Hamiltonians of the designed sensors were time-independent. We have conducted a thorough investigation into various features associated with optimal conditions for sensitivity enhancement, such as the optimal timing window for achieving high sensitivity using the energy spectrum of eigenvalues and the population distribution of eigenstates. Notably, we have demonstrated that when the time-evolution trajectory of the system approaches the EP, both eigenvalue-based and eigenstate-based quantum sensors exhibit significant enhancements in sensitivity, 9.21-fold and 50-fold, respectively, compared to conventional Hermitian sensors. Moreover, we emphasize that the eigenstate-based sensor still demonstrates divergent susceptibility even when the system's time-evolution trajectory deviates from the EP (for details, see Appendix A). However, there is a trade-off between achieving high sensitivity (through a small perturbation λ) and ensuring the reliability of quantum sensing measurements (with a low uncertainty ratio $\Delta\lambda'/\lambda$ for the perturbation), especially when considering the effects of background noise and the limitations of practical measurements (for more details, see Appendices B and C). Our findings pave a novel pathway for advanced sensing in a time-sensitive framework, thereby complementing ongoing efforts to leverage the distinctive properties of open systems.

The presented results are not only applicable to single-qubit NH systems, but also can be extended to time-modulated multi-mode NH systems that dynamically encircle an EP or DP [39, 42]. In this context, multi-mode systems with higher-order EPs or multiple low-order EPs may exhibit more complex and novel phenomena. Moreover, extending this work to explore sensors in time-dependent open quantum systems, based on the exceptional points within the hybrid-Liouvillian formalism [58, 59], represents a promising direction for future research. Additionally, by considering applications in multiple sensing scenarios over a time sequence and integrating other enhancement methods, such as exceptional surfaces [51], the EP shift sensing mechanism [52], and the linewidth broadening mechanism [53], the performance of sensors can be further enhanced, which also represents a promising direction for future research.

ACKNOWLEDGEMENT

This work was supported by National Key Research and Development Program of China (Grant No. 2024YFA1408900), National Natural Science Foundation of China (NSFC) (Grants Nos. 12264040, 12374333, 12364048 and U21A20436), Jiangxi Natural Science Foundation (Grant Nos. 20232BCJ23022 and 20242BAB25037), Innovation Program for Quantum Science and Technology (Grant No. 2021ZD0301705), and Jiangxi Province Key Laboratory of Applied Optical Technology (Grant No. 2024SSY03051).

Appendix A: The impact of distancing from an exceptional point

In the main text, we have examined the performance of the quantum sensor near the EP. Here, we briefly analyze the performance of the scheme when the time-evolution trajectory of the system is situated away from the EP. Without loss of generality, the time-evolution trajectory of the system follows that depicted by Eq. (13), with the parameters set as $g_0 = 0.02$, $\Delta_0 = 0.04$, $\Gamma_0 = 0.1$, $\omega = \pi$, and $\alpha = -1$. Additionally, as discussed in Section IIIA, the parameter $|\Delta_E(\tau)|_{\min}$ serves as an indicator used to evaluate the extent to which the trajectory of the system parameters deviates from the EP or DP.

For the eigenvalue-based quantum sensor, as indicated in Eq. (7), the susceptibility of the quantum sensor is contingent upon the eigenvalue-matching condition ($\Delta_E(\tau) \rightarrow 0$ near the EP or DP). By comparing Figs. 2 and 3 with Fig. 8(a), it is evident that both the susceptibility $|\chi|$ and the sensitivity enhancement factor S_E of the quantum sensor diminish significantly when the time-evolution trajectory of the system is distant from the EP, specifically when $|\Delta_E(\tau)|_{\min} > 0.02$. However, by comparing Figs. 5 and 7 with Fig. 8(b), it becomes clear that for the eigenstate-based quantum sensor, a relatively high susceptibility $|\chi_H(t, \lambda)|_{\max} = 25$ is still observed. Moreover, the non-Hermiticity-enhanced susceptibility S_P exceeds 20 over a wide range of parameters. Consequently, the eigenstate-based sensor exhibits significant susceptibility during dynamical evolution, even when not close to an EP.

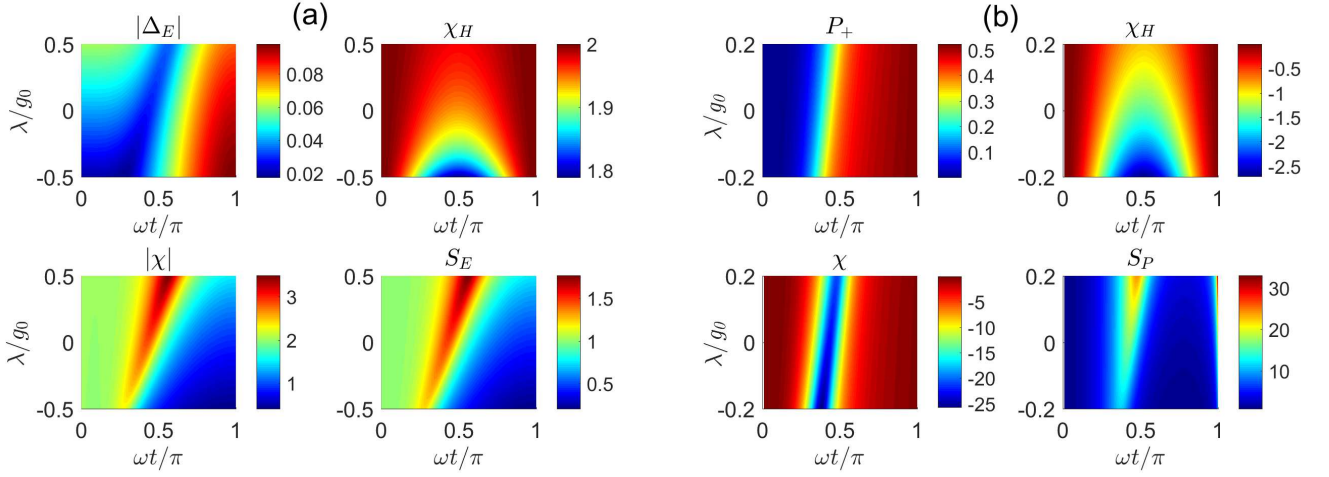


FIG. 8: (a) The parameters $|\Delta_E|$, $|\chi|$, χ_H , and S_E are analyzed as functions of λ/g_0 and t for the eigenvalue-based quantum sensor. (b) For the eigenstate-based quantum sensor, the parameters P_+ , χ , χ_H , and S_P are analyzed as functions of λ/g_0 and t . Other parameters are set to $g_0 = 0.02$, $\Delta_0 = 0.04$, $\Gamma_0 = 0.1$, $\omega = \pi$, and $\alpha = -1$.

Appendix B: Quantum sensing under noise

Noise represents a fundamental challenge for sensors, as the performance of a sensor is ultimately constrained by noise [11]. Without loss of generality, we now proceed to analyze the performance of the eigenstate-based sensor while taking into account both background noise and the imperfections inherent in actual measurements.

Under the combined effects of background noise and the imperfections in actual measurements, the measured population of the right eigenstate in Eq. (17) is accordingly modified as [11]

$$\begin{aligned}
P'_+(t, \lambda) &= \frac{N_+(t, \lambda) + N'_+(t, \lambda)}{N_+(t, \lambda) + N'_+(t, \lambda) + N_-(t, \lambda) + N'_-(t, \lambda)} \\
&= \frac{N_+(t, \lambda)}{N_+(t, \lambda) + N_-(t, \lambda)} \frac{1 + \frac{N'_+(t, \lambda)}{N_+(t, \lambda)}}{1 + \frac{N'_+(t, \lambda) + N'_-(t, \lambda)}{N_+(t, \lambda) + N_-(t, \lambda)}} \\
&\approx \frac{N_+(t, \lambda)}{N_+(t, \lambda) + N_-(t, \lambda)} \left[1 + \frac{N'_+(t, \lambda)}{N_+(t, \lambda)}\right] \left[1 - \frac{N'_+(t, \lambda) + N'_-(t, \lambda)}{N_+(t, \lambda) + N_-(t, \lambda)}\right] \\
&\approx \frac{N_+(t, \lambda)}{N_+(t, \lambda) + N_-(t, \lambda)} \left[1 + \frac{N'_+(t, \lambda)}{N_+(t, \lambda)} - \frac{N'_+(t, \lambda) + N'_-(t, \lambda)}{N_+(t, \lambda) + N_-(t, \lambda)}\right] \\
&= P_+(t, \lambda) + [1 - P_+(t, \lambda)] \frac{N'_+(t, \lambda)}{N} - P_+(t, \lambda) \frac{N'_-(t, \lambda)}{N},
\end{aligned} \tag{B1}$$

where $N_m(t, \lambda) = |\langle \hat{\phi}_m(t, \lambda) | \Psi(t) \rangle|^2$ ($m = +, -$), $N'_m(t, \lambda)$ quantify the additional noisy contributions to the corresponding eigenstate populations caused by background noise, and $N = N_+(t, \lambda) + N_-(t, \lambda)$. Here, we assume that $\frac{1}{1 + \frac{N'_+(t, \lambda) + N'_-(t, \lambda)}{N_+(t, \lambda) + N_-(t, \lambda)}} \approx 1 - \frac{N'_+(t, \lambda) + N'_-(t, \lambda)}{N_+(t, \lambda) + N_-(t, \lambda)}$ when $\frac{N'_+(t, \lambda) + N'_-(t, \lambda)}{N_+(t, \lambda) + N_-(t, \lambda)} \ll 1$. In general, background noise is completely random.

The corresponding population results are assumed to be uniformly distributed within the intervals $N'_+(t, \lambda) \in [0, \eta_+ N]$ and $N'_-(t, \lambda) \in [0, \eta_- N]$, respectively. However, one can fix the average values of η_+ and η_- by performing repetitive measurements with the same apparatus.

Then, by applying the error propagation procedure to Eq. (B1), the measurement noise of $P'_+(t, \lambda)$ can be determined as

$$\begin{aligned}
\Delta P'^2_+(t, \lambda) &= \left[\frac{\partial P'_+(t, \lambda)}{\partial P_+(t, \lambda)} \Delta P_+(t, \lambda) \right]^2 + \left[\frac{\partial P'_+(t, \lambda)}{\partial N'_+(t, \lambda)/N} \Delta \frac{N'_+(t, \lambda)}{N} \right]^2 + \left[\frac{\partial P'_+(t, \lambda)}{\partial N'_-(t, \lambda)/N} \Delta \frac{N'_-(t, \lambda)}{N} \right]^2 \\
&= [1 - (\eta_+ + \eta_-)]^2 \Delta P^2_+(t, \lambda) + \{ [1 - P_+(t, \lambda)]^2 \eta_+^2 + P_+^2(t, \lambda) \eta_-^2 \},
\end{aligned} \tag{B2}$$

where $\Delta P^2_+(t, \lambda) = \frac{P_+^2(t, \lambda) \Delta P^2(t, \lambda) + P_-^2(t, \lambda) \Delta P^2_-(t, \lambda)}{N^4}$ is the standard deviation for the quantum sensor, arising from the fluctuations in population measurements and can be averaged out through repetitive measurements. Therefore,

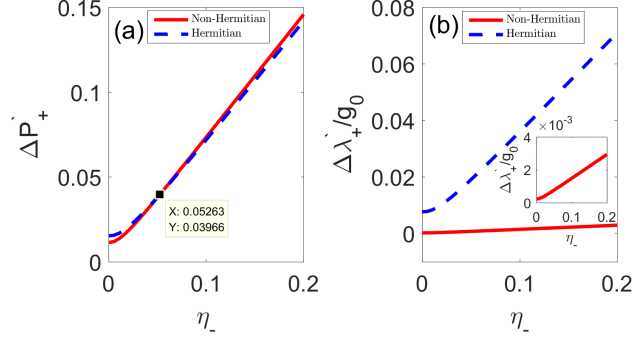


FIG. 9: (a) The standard deviation of $\Delta P'_+$ as a function of η_- . (b) The standard deviation of $\Delta\lambda'$ as a function of η_- . The red curves denote the non-Hermitian sensor, while the blue curves represent the results of its Hermitian counterpart. We choose the working point of the sensor in Fig. 7, i.e., $\lambda/g_0 = -0.618$, $S_P = 49.97$ when $t = 0.98\pi/\omega$. The population $P_+ = 0.3784$ for the non-Hermitian sensor and $P_+ = 0.49$ for its Hermitian counterpart. Other parameters are set to $\eta_+ = \eta_-$, $\Delta P_+ = P_+ \times 3\%$.

the first term on the right-hand side of Eq. (B2) may tend to zero with sufficiently many repetitive measurements. However, the second term is independent of the fluctuations in population measurements and cannot be averaged out, as it originates from background noise. Based on the above analysis, we can approximate the minimum measurement uncertainty of the estimated parameter as follows:

$$\Delta\lambda' = \frac{\Delta P'_+(t, \lambda)}{|\partial_{\lambda'} P'_+(t, \lambda)|} \leq \frac{\Delta P'_+(t, \lambda)}{|[1 - (\eta_+ + \eta_-)] \partial_{\lambda} P_+(t, \lambda)|} \geq \frac{\Delta P'_+(t, \lambda)}{|\chi(t, \lambda)|}, \quad (\text{B3})$$

with $(\eta_+ + \eta_-) \ll 1$, i.e., $\text{Min}[\Delta\lambda'] \approx \Delta P'_+(t, \lambda)/|\chi(t, \lambda)|$.

Without loss of generality, we choose the working point of the sensor in Fig. 7, i.e., $\lambda/g_0 = -0.618$, $S_P = 49.97$ when $t = 0.98\pi/\omega$. Then, in Fig. 9, we illustrate the dependence of the measurement uncertainties $\Delta P'_+$ and $\Delta\lambda'$ on the noise strength η_- (assuming for simplicity that $\eta_+ = \eta_-$) for both non-Hermitian and Hermitian sensors. The results reveal that for $\eta_- \leq 0.05263$, the uncertainty $\Delta P'_+$ of the non-Hermitian sensor is slightly lower than that of the Hermitian sensor. Conversely, when $\eta_- \geq 0.05263$, the uncertainty $\Delta P'_+$ of the non-Hermitian sensor becomes slightly higher than that of the Hermitian sensor. Nevertheless, the minimum value of $\Delta\lambda'$ for the non-Hermitian sensor consistently remains smaller than that of the Hermitian sensor. Consequently, the non-Hermitian sensor demonstrates superior performance relative to its Hermitian counterpart, achieving reduced measurement uncertainties in both the presence and absence of background noise.

Moreover, ideally, the enhancement of the sensor can reach an extremely high value when the perturbation λ becomes exceedingly small at a specific time, as illustrated in Figs. 5 and 7. In practice, however, this theoretical prediction is not feasible in actual experimental measurements. Specifically, as shown in Fig. 9 (b), the magnitude of the uncertainty $\Delta\lambda'$ is on the order of $10^{-3}g_0$, even with a relatively large background noise intensity ($\eta_+ = \eta_- = 0.05$). This suggests that the true value of the parameter λ selected for measurement should ideally be around $10^{-2}g_0$; otherwise, the excessively large uncertainty $\Delta\lambda'$ may compromise the physical significance of the measurement. Of course, the uncertainty of $\Delta\lambda'$ could be further reduced if the intensity of background noise were decreased further. However, in some experimental scenarios, achieving very low background noise intensity remains a significant challenge. Therefore, there exists a trade-off between achieving high sensitivity (via a small perturbation λ) and ensuring the reliability of quantum sensing measurements (with a low uncertainty ratio $\Delta\lambda'/\lambda$ for the perturbation), particularly when accounting for the impact of background noise and the constraints of practical measurements.

Appendix C: Quantum sensing based on the master equation

In the main text, Eq. (14) describes the evolution of the system under an effective non-Hermitian Hamiltonian, which represents a partial scenario of open quantum system dynamics (in the absence of quantum jumps). Generally, the complete dynamics of the system is governed by the following Markovian master equation (with $\hbar = 1$)

$$\begin{aligned} \dot{\rho}(t) &= -i[H_0(t) + \lambda\sigma_x, \rho(t)] + \mathcal{L}[\rho(t)], \\ \mathcal{L}[\rho(t)] &= \gamma(t)[\sigma_- \rho(t) \sigma_+ - \frac{1}{2}\{\sigma_+ \sigma_-, \rho(t)\}], \end{aligned} \quad (\text{C1})$$

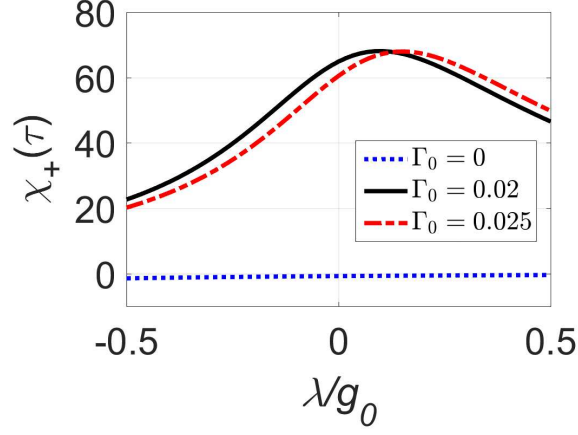


FIG. 10: The susceptibility $\chi(\tau)$ of the quantum sensing based on the master equation as functions of λ/g_0 under different dissipation coefficients Γ_0 . Other parameters are set to $\tau = 0.98\pi/\omega$, $g_0 = 0.01$, $\Delta_0 = 0.04$, and $\alpha = -1$.

with $\gamma_+(t) = -\gamma_-(t) = \gamma(t) = \Gamma_0 \sin^2(\frac{\omega t}{2})$. In this case, the quantum state of the system is generally a mixed state, which differs from that described in Eq. (14). The population of the right eigenstate is accordingly modified as

$$P_+(t, \lambda) = \langle \widehat{\phi}_+(t, \lambda) | \rho(t) | \phi_+(t, \lambda) \rangle. \quad (\text{C2})$$

The above master equation is not easily solvable analytically; therefore, we conduct a detailed numerical analysis, as shown in Fig. 10. The numerical results indicate that the quantum sensor still exhibits superior performance compared to its Hermitian counterpart ($\Gamma_0 = 0$), achieving high susceptibility χ over a broad range of parameters. Furthermore, variations in the dissipation coefficient can also alter the system's sensitivity to some extent.

-
- [1] C. M. Bender and S. Boettcher, Real Spectra in Non-Hermitian Hamiltonians Having PT Symmetry, *Phys. Rev. Lett.* **80**, 5243 (1998).
 - [2] W. D. Heiss, Repulsion of resonance states and exceptional points, *Phys. Rev. E* **61**, 929 (2000).
 - [3] H. Cartarius, J. Main, and G. Wunner, Exceptional points in atomic spectra, *Phys. Rev. Lett.* **99**, 173003 (2007).
 - [4] L. Feng, R. El-Ganainy and L. Ge, Non-Hermitian photonics based on parity-time symmetry, *Nat. Photon.* **11**, 752 (2017).
 - [5] B. Peng, S. K. Özdemir, F. Lei, F. Monifi, M. Gianfreda, G. L. Long, S. Fan, F. Nori, C. M. Bender, and L. Yang, Parity-timesymmetric whispering-gallery microcavities, *Nat. Phys.* **10**, 394 (2014).
 - [6] Y. Ashida, Z. Gong, and M. Ueda, Non-Hermitian physics, *Adv. Phys.* **69**, 249 (2020).
 - [7] Q. C. Wu, J. L. Zhao, Y. L. Fang, Y. Zhang, D. X. Chen, C. P. Yang and F. Nori, Extension of Noether's theorem in PT-symmetry systems and its experimental demonstration in an optical setup, *Sci. China-Phys. Mech. Astron.* **66**(4), 240312 (2023).
 - [8] E. J. Bergholtz, J. C. Budich, and F. K. Kunst, Exceptional topology of non-Hermitian systems, *Rev. Mod. Phys.* **93**, 015005 (2021).
 - [9] C. Guria, Q. Zhong, Ş. K. Özdemir, Y. S. S. Patil, R. El-Ganainy, and J. G. Emmet Harris, Resolving the topology of encircling multiple exceptional points, *Nat. Commun.* **15**, 1369 (2024).
 - [10] A. C. Tam, Applications of photoacoustic sensing techniques, *Rev. Mod. Phys.* **58**, 381 (1986).
 - [11] C. L. Degen, F. Reinhard, and P. Cappellaro, Quantum sensing, *Rev. Mod. Phys.* **89**, 035002 (2017).
 - [12] M. Z. Zhang, W. Sweeney, C. W. Hsu, L. Yang, A. D. Stone, and L. Jiang, Quantum Noise Theory of Exceptional Point Sensors, *Phys. Rev. Lett.* **123**, 180501 (2019).
 - [13] J. Wiersig, Prospects and fundamental limits in exceptional point-based sensing, *Nat. Commun.* **11**, 2454 (2020).
 - [14] X. W. Luo, C. W. Zhang, and S. W. Du, Quantum squeezing and sensing with pseudo-anti-parity-time symmetry, *Phys. Rev. Lett.* **128**, 173602 (2022).
 - [15] W. C. Wong and J. S. Li, Exceptional-point sensing with a quantum interferometer, *New J. Phys.* **25**, 033018 (2023).
 - [16] J. N. Li, H. D. Liu, Z. H. Wang, and X. X. Yi, Enhanced parameter estimation by measurement of non-Hermitian operators, *AAPPS Bulletin* **33**, 22 (2023).
 - [17] X. K. Wei, C. L. Ren, B. W. Liu, Y. Peng, and S. L. Zhuang, The theory, technology, and application of terahertz metamaterial biosensors: a review, *Fundamental Research* **5**, 571 (2025).
 - [18] H. Xu, X. K. Song, D. Wang, and L. Ye, Quantum sensing of control errors in three-level systems by coherent control techniques, *Sci. China-Phys. Mech. Astron.* **66**(4), 240314 (2023).

- [19] Y. C. Liu, Y. B. Cheng, X. B. Pan, Z. Z. Sun, D. Pan, and G. L. Long, Quantum integrated sensing and communication via entanglement, *Phys. Rev. Applied* **22**(3), 034051 (2024).
- [20] H. Hodaei, A. U. Hassan, S. Wittek, H. Garcia-Gracia, R. El-Ganainy, D. N. Christodoulides, and M. Khajavikhan, Enhanced sensitivity at higher-order exceptional points, *Nature* **548**, 187 (2017).
- [21] W. J. Chen, Ş. Özdemir, G. Zhao, J. Wiersig, and L. Yang, Exceptional points enhance sensing in an optical microcavity, *Nature (London)* **548**, 192 (2017).
- [22] M. V. Berry, Physics of nonhermitian degeneracies, *Czech. J. Phys.* **54**, 1039 (2004).
- [23] W. D. Heiss, The physics of exceptional points, *J. Phys. A* **45**, 444016 (2012).
- [24] J. Wiersig, Enhancing the sensitivity of frequency and energy splitting detection by using exceptional points: Application to microcavity sensors for single-particle detection, *Phys. Rev. Lett.* **112**, 203901 (2014).
- [25] R. Fleury, D. Sounas, and A. Alù, An invisible acoustic sensor based on parity-time symmetry, *Nat. Commun.* **6**, 5905 (2015).
- [26] Y. H. Lai, Y. K. Lu, M. G. Suh, Z. Q. Yuan, and K. Vahala, Observation of the exceptional-point-enhanced Sagnac effect, *Nature (London)* **576**, 65 (2019).
- [27] L. Y. Ding, K. Y. Shi, Q. X. Zhang, D. N. Shen, X. Zhang, and W. Zhang, Experimental determination of PT-symmetric exceptional points in a single trapped ion, *Phys. Rev. Lett.* **126**, 083604 (2021).
- [28] Y. Wu, W. Q. Liu, J. P. Geng, X. R. Song, X. Y. Ye, C. K. Duan, X. Rong, and J. F. Du, Observation of parity-time symmetry breaking in a single-spin system, *Science* **364**, 878 (2019).
- [29] S. Yu, Y. Meng, J. S. Tang, X. Y. Xu, Y. T. Wang, P. Yin, Z. J. Ke, W. Liu, Z. P. Li, Y. Z. Yang, G. Chen, Y. J. Han, C. F. Li, and G. C. Guo, Experimental investigation of quantum PT-enhanced sensor, *Phys. Rev. Lett.* **125**, 240506 (2020).
- [30] P. R. Han, F. Wu, X. J. Huang, H. Z. Wu, C. L. Zou, W. Yi, M. Z. Zhang, H. K. Li, K. Xu, D. N. Zheng, H. Fan, J. M. Wen, Z. B. Yang and S. B. Zheng, Enhancement of sensitivity near exceptional points in dissipative qubit-resonator systems, *Advanced Quantum Technologies*, 2400446 (2025).
- [31] Y. M. Chu, Y. Liu, H. B. Liu, and J. M. Cai, Quantum sensing with a single-qubit pseudo-hermitian system, *Phys. Rev. Lett.* **124**, 020501 (2020).
- [32] L. Xiao, Y. M. Chu, Q. Lin, H. Q. Lin, W. Yi, J. M. Cai, and P. Xue, Non-Hermitian sensing in the absence of exceptional points, *Phys. Rev. Lett.* **124**, 020501 (2024).
- [33] A. U. Hassan, B. Zhen, M. Soljačić, M. Khajavikhan, and D. N. Christodoulides, Dynamically encircling exceptional points: Exact evolution and polarization state conversion, *Phys. Rev. Lett.* **118**, 093002 (2017).
- [34] A. Li, J. Dong, J. Wang, Z. Cheng, J. S. Ho, D. Zhang, et al., Hamiltonian hopping for efficient chiral mode switching in encircling exceptional points, *Phys. Rev. Lett.* **125**(18), 187403 (2020).
- [35] Q. C. Wu, Y. H. Zhou, B. L. Ye, T. Liu and C. P. Yang, Nonadiabatic quantum state engineering by time-dependent decoherence-free subspaces in open quantum systems, *New J. Phys.* **23**, 113005 (2021).
- [36] J. Doppler, A. A. Mailybaev, J. Böhm, U. Kuhl, A. Girschik, F. Libisch, T. J. Milburn, P. Rabl, N. Moiseyev, and S. Rotter, Dynamically encircling an exceptional point for asymmetric mode switching, *Nature (London)* **537**, 76 (2016).
- [37] I. I. Arkhipov, A. Miranowicz, F. Minganti, Ş. Özdemir, and F. Nori, Restoring adiabatic state transfer in time-modulated non-hermitian systems, *Phys. Rev. Lett.* **133**, 113802, (2024)
- [38] Q. C. Wu, J. L. Zhao, Y. H. Zhou, B. L. Ye, Y. L. Fang, Z. W., Zhou and C. P. Yang, Shortcuts to adiabatic state transfer in time-modulated two-level non-Hermitian systems, *Phys. Rev. A* **111**, 022410 (2025).
- [39] S. Khandelwal, W. J. Chen, K. W. Murch, and G. Haack, Chiral Bell-state transfer via dissipative liouvillian dynamics, *Phys. Rev. Lett.* **133**, 070403 (2024).
- [40] J. Feilhauer, A. Schumer, J. Doppler, A. A. Mailybaev, J. Böhm, U. Kuhl, N. Moiseyev, and S. Rotter, Encircling exceptional points as a non-Hermitian extension of rapid adiabatic passage, *Phys. Rev. A* **102**, 040201 (2020).
- [41] M. S. Ergoktas, S. Soleymani, N. Kakenov, K. Wang, T. B. Smith, G. Bakan, S. Balci, A. Principi, K. S. Novoselov, S. K. Ozdemir, and C. Kocabas, Topological engineering of terahertz light using electrically tunable exceptional point singularities, *Science* **376**, 184 (2022).
- [42] I. I. Arkhipov, A. Miranowicz, F. Minganti, Ş. Özdemir, and F. Nori, Dynamically crossing diabolic points while encircling exceptional curves: A programmable symmetric/asymmetric multimode switch, *Nat. Commun.* **14**, 2076 (2023).
- [43] Z. Tang, T. Chen, and X. Zhang, Highly efficient transfer of quantum state and robust generation of entanglement state around exceptional lines, *Laser Photonics Rev.* 2300794 (2023).
- [44] H. Nasari, G. L. Galmiche, H. E. L. Aviles, A. Schumer, A. U. Hassan, Q. Zhong, S. Rotter, P. LiKamWa, D. N. Christodoulides, and M. Khajavikhan, Observation of chiral state transfer without encircling an exceptional point, *Nature* **605**, 256 (2022).
- [45] Q. C. Wu, Y. L. Fang, Y. H. Zhou, J. L. Zhao, Y. H. Kang, Q. P. Su, and C. P. Yang, Efficient and controlled symmetric and asymmetric Bell-state transfers in a dissipative Jaynes-Cummings model, *arXiv preprint arXiv:2411.10812* (2024).
- [46] W. Chen, Ş. Özdemir, G. Zhao, J. Wiersig, and L. Yang, Exceptional points enhance sensing in an optical microcavity, *Nature (London)* **548**, 192 (2017).
- [47] I. I. Arkhipov, A. Miranowicz, F. Nori, Ş. K. Özdemir, and F. Minganti, Fully solvable finite simplex lattices with open boundaries in arbitrary dimensions, *Phys. Rev. Res.* **5**, 043092 (2023).
- [48] H. S. Xu and L. Jin, Coupling-induced nonunitary and unitary scattering in anti-PT-symmetric non-Hermitian systems, *Phys. Rev. A* **104**, 012218 (2021).
- [49] Y. Wu, W. Q. Liu, J. P. Geng, X. R. Song, X. Y. Ye, C. K. Duan, X. Rong, and J. F. Du, Observation of parity-time symmetry breaking in a single-spin system, *Science* **364**, 878 (2019).

- [50] L. Xiao, K. K. Wang, X. Zhan, Z.-H. Bian, K. Kawabata, M. Ueda, W. Yi, and P. Xue, Observation of critical phenomena in parity-time-symmetric quantum dynamics, *Phys. Rev. Lett.* **123**, 230401 (2019).
- [51] G. Q. Qin, R. R. Xie, H. Zhang, Y. Q. Hu, M. Wang, G. Q. Li, H. Xu, F. Lei, D. Ruan, and G. L. Long, Experimental realization of sensitivity enhancement and suppression with exceptional surfaces, *Laser Photonics Rev.* **15**(5), 2000569 (2021).
- [52] X. Mao, G. Q. Qin, H. Zhang, B. Y. Wang, D. Long, G. Q. Li, and G. L. Long, Enhanced sensing mechanism based on shifting an exceptional point, *Research* **6**, 0260 (2023).
- [53] D. Long, J. D. Zhu, X. Mao, G. Q. Qin, M. Wang, G. Q. Li, F. Bo, and G. L. Long, Exceptional-point-enhanced nanoparticle sensor utilizing a linewidth broadening mechanism, *Opt. Lett.* **50**, 852-855 (2025).
- [54] A. Chefles and S. M. Barnett, Strategies for discriminating between non-orthogonal quantum states. *Journal of Modern Optics*, **45**(6), 1295-1302 (1998).
- [55] J. A. Bergou, U. Herzog, and M. Hillery, Discrimination of Quantum States, in *Quantum state estimation*, Lecture Notes in Physics, **649**, 417-465 (Springer, Berlin, Heidelberg, 2004).
- [56] B. X. Tian, W. Z. Yan, Z. B. Hou, G. Y. Xiang, C. F. Li, and G. C. Guo, Minimum-consumption discrimination of quantum states via globally optimal adaptive measurements, *Phys. Rev. Lett.* **132**, 110801 (2024).
- [57] D. X. Chen, Y. Zhang, J. L. Zhao, Q. C. Wu, Y. L. Fang, C. P. Yang, and F. Nori, Quantum state discrimination in a PT-symmetric system, *Phys. Rev. A* **106**, 022438 (2022).
- [58] F. Minganti, A. Miranowicz, R. W. Chhajlany, I. I. Arkhipov, and F. Nori, Hybrid-Liouvilian formalism connecting exceptional points of non-Hermitian Hamiltonians and Liouvillians via postselection of quantum trajectories, *Phys. Rev. A* **101**, 062112 (2020).
- [59] K. H. Sun and W. Yi, Encircling the Liouvillian exceptional points: a brief review, *AAPPS Bulletin* **34**(1), 22 (2024).